To cite this version :

Mohammad AHMADIFAR, Khaled BENFRIHA, Mohammadali SHIRINBAYAN, Améziane AOUSSAT, Joseph FITOUSSI - Exploring fatigue characteristics of metallic boss-polymer liner adhesion in hydrogen storage tanks: Experimental insights post surface treatment - Journal of Energy Storage - Vol. 75, p.109771 - 2023

Exploring fatigue characteristics of metallic boss-polymer liner adhesion in hydrogen storage tanks: Experimental insights post surface treatment

M. Ahmadifar [a,b,*], K. Benfriha [a], M. Shirinbayan [b], A. Aoussat [a], J. Fitoussi [b]

[a] *Arts et Metiers Institute of Technology, CNAM, LCPI, HESAM University, F-75013 Paris, France*
[b] *Arts et Metiers Institute of Technology, CNAM, PIMM, HESAM University, F-75013 Paris, France*

ARTICLE INFO

ABSTRACT

Progress in hydrogen fuel powered systems has been propelled by the implementation of secure, reliable, and cost-effective hydrogen storage and transportation technologies. The fourth category, distinguished by a polymer liner serving as a hydrogen diffusion barrier, fully encapsulated within a fiber-reinforced composite to bestow structural integrity, has garnered substantial attention from the automotive industry due to its lightweight nature and rational manufacturing process. The method of rotomolding has sparked interest among manufacturers due to its capability to directly bond the metallic component to the polymer substrate, specifically the liner, thus negating the need for welding and its attendant imperfections. In fact, a pivotal facet of fourth-generation hydrogen storage systems revolves around the interface connection between the polymer liner and the metallic boss, posing as a structural Achilles' heel. For the study's purposes, a scaled-down demonstrator was fabricated using rotomolding in which a nozzle-liner interface mimics the boss-liner interface of the actual system. This demonstrator was designed to facilitate the mechanical characterization of the interface under quasi-static and fatigue loading. The thermal cycling phases of rotational molding and the surface treatments undertaken have been optimized in order to enhance direct adhesion within the metal-polymer interface. This study commences by assessing the efficacy of two treatments (sandblasting and flaming) applied to the aluminum nozzle surface. Subsequently, we explore the adhesion microstructural and mechanical characteristics of the treated nozzle onto a medium-density polyethylene polymer (liner). Lastly, we delve into an exploration of the damage and fatigue behaviors endemic to the metal-polymer interface region. The obtained Wöhler curves disclose a linear trend for the metal-polymer interface. Moreover, the metal-polymer interface evinces heightened resilience against damage and fracture for sandblasted interfaces. This inquiry underscores the potency of innovative polymer-metal interfaces treatment in amplifying the reliability and robustness of hydrogen storage technology.

1. Introduction

As an alternative to conventional energy sources, compressed natural gas (CNG) and hydrogen are becoming more and more popular [1,2]. In recent years, hydrogen has attracted considerable attention as a clean fuel. Therefore, hydrogen storage methods have been developed in response to this demand. In order to develop hydrogen storage and transportation technology, storage tanks are essential [3–6].

A hydrogen vessel can be classified into four major types, which are Type I, Type II, Type III, and Type IV (Table 1), [7–14] which are:

Vehicles are one of the most common applications of hydrogen vessels. Table 1 lists the specific features of each type of hydrogen vessel. While type III hydrogen tanks exhibited some weaknesses compared the type IV in the case of vehicle application such as; economy, weight, and efficiency [3,15,16]. Type IV hydrogen tanks have a plastic barrier layer, which has many advantages over type III hydrogen tanks, including low cost, corrosion resistance, fatigue resistance, durability, and lightweight [3,17–19]. Indeed, type IV hydrogen tanks are composed a polymer liner, the outer layer which is carbon fiber composite, and the metallic nozzle (Fig. 1). The polymer liner prevents hydrogen permeation. The carbon fiber composite layer increases the mechanical strength of the manufactured tank [20–23]. Moreover, hydrogen gas is loaded into the

Table 1
Types/generations and the related features of the hydrogen storage tanks.

Type	Composition	Features	Function
Type I		- Heavy weight - Corrosion probability	Hydrogen gas storage
Type II		- Heavy weight - Short-term service caused by internal corrosion	
Type III		- Light weight - No permeation - Galvanic corrosion probability between liner and fiber - Endurance of the high burst pressure	
Type IV		- Light weight - lower burst pressure - Manufactured simply - Probability of the permeation through liner - An easy-to-manufacture product	
Type V		- Recyclability - Light weight - An easy-to-manufacture product	

- **Type I:** Metallic vessels.
- **Type II:** Thick metallic liner hoop wrapped with a fiber-resin composite.
- **Type III:** Metallic liner fully wrapped with fiber-resin composite.
- **Type IV:** Polymer liner fully wrapped with fiber-resin composite.
- **Type V:** Liner-less vessel with a full composite shell.

tank through the metallic nozzle.

Considering that hydrogen is highly permeabilized and extremely high pressure exists in type IV high-pressure storage vessels, the interface between the liner polymer layer and the metallic nozzle is a certainly critical section. Thus, hydrogen would be most likely to diffuse from this location. Therefore, the interface between the polymer liner and metallic nozzle continues to be one of the major weaknesses of the type IV high-pressure vessels, despite the extensive studies. There are a lot of investigations being conducted for obtaining better Metal-Polymer adhesion properties by applying different techniques [24–27].

The two common methods of the manufacturing polymer liners are extrusion blow-molding and rotational molding. The metallic nozzle is welded to the polymer (liner section of the manufactured hydrogen pressure vessel) during the extrusion process. While in the rotomolding process, the metallic nozzle will be positioned directly in the mold and adhered to the polymer prior to the wrapping process of the carbon fiber composite layer. Consequently, rotational molding has captivated manufacturers' attention due to its ability for the direct adhesion of the metallic nozzle and the polymer layer (liner section) simultaneously, without welding and its subsequent process defects [28–30].

Rotomolding or rotational molding process is one of the most developed techniques utilized for processing thermoplastic polymers to manufacture large-scale products [31–33]. Rotomolding provides the possibility of manufacturing the almost waste-free shaping of thin-walled parts with favorable characterizations. In fact, rotational molding enables the manufacture of hollow and seamless objects with complex geometries [34,35]. Rotational molding process consists of four steps (Table 2). In the first step, a specific amount of raw material is poured into the designed mold. Following the filling process, the filled mold will be simultaneously heated and rotated in orthogonal axes (second step). Hot air convection is the most common method for heating rotational molds, while infrared and hot liquid can also be utilized. Indeed, the plastic charge inside the mold melts due to heat transfer and coats the interior uniformly. As the third step, the mold is moved to a cooling station as the biaxial rotation proceeds. To solidify the required part, either air, water, or a combination of both will be utilized for cooling. Finally, upon opening the mold, the manufactured part will be removed (step four).

A variety of adhesion theories have been proposed over the years, which include chemical bonding principle [36], diffusion principle [37], electrostatic (contact charging) theory [36], wetting (adsorption) theory [38,39], and mechanical interlocking theory [40,41]. Based on these theories, the parameters that contribute to the adhesion between two materials can influence the properties of the interface between them and increase the adhesion, consequently [42–46].

The purpose of the present study is to analyze the efficiency of two surface treatments on the metallic section of the manufactured hydrogen storage tanks (nozzles) in order to evaluate the possibility of selecting the most appropriate treatment or a combination thereof. The two
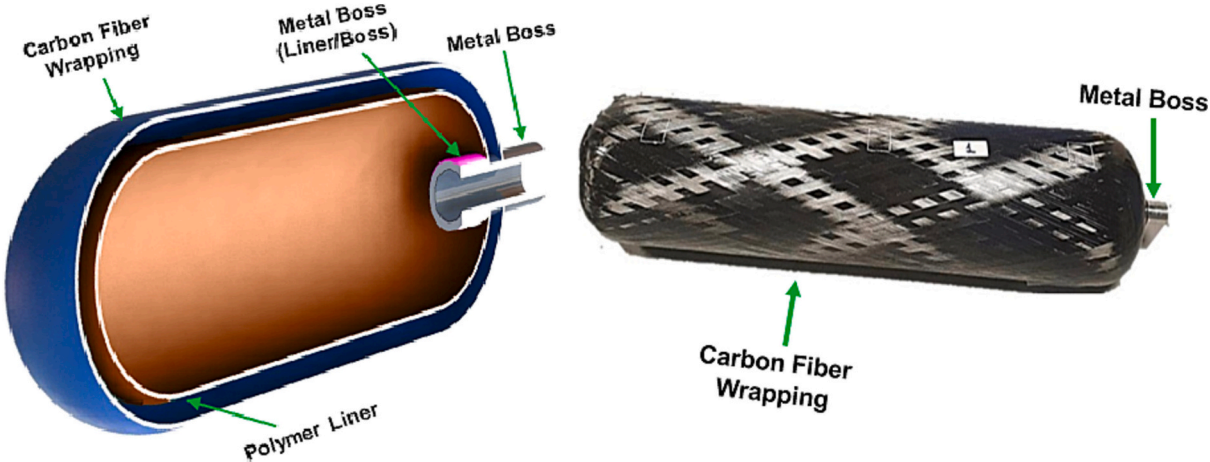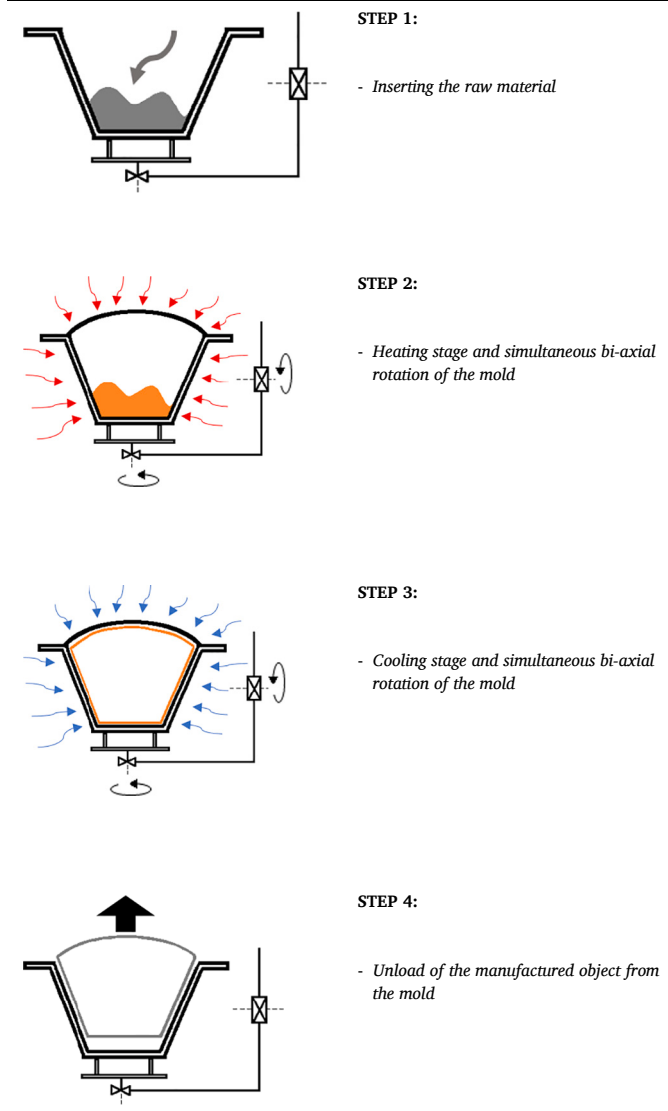

Fig. 1. Type IV hydrogen pressure vessel.

Table 2
The sequences of the manufacturing process by rotomolding.

	STEP 1: - *Inserting the raw material*
	STEP 2: - *Heating stage and simultaneous bi-axial rotation of the mold*
	STEP 3: - *Cooling stage and simultaneous bi-axial rotation of the mold*
	STEP 4: - *Unload of the manufactured object from the mold*

selected surface treatments which were based on the mechanical interlocking of the Metal-Polymer were sandblasting and flaming of the metallic nozzles before the rotomolding manufacturing process. The selection of these treatments was based on their ease of application and speed of implementation. As was stated above, the manufactured type IV hydrogen storage tanks by rotomolding, are constituted of an inner layer (polymer), a metallic nozzle, a fiber-resin composite layer, and a Metal-Polymer interface. The focus of this study will be on the interface of the liner polymer layer and the metallic nozzle (Metal-Polymer) section. Therefore, the efficiency of the selected treatments on the direct adhesion of the Metal-Polymer interface in the manufactured scaled-down hydrogen storage tank demonstrators by rotomolding was evaluated by the designed apparent shear test. Finally, the fatigue and consequently damage behaviors of the manufactured storage tank demonstrator with the most suitable surface treatment (based on the conducted studies) were studied as an investigation of the features and durability of the related interface during the service.

2. Materials and methods

Concerning the execution of this research project, the below chart

(Fig. 2) has been developed in order to outline the related sequences. The sandblasting and flame as the surface treatments were performed on the metallic nozzle. The efficiency of the different parameters of these treatments on the direct adhesion of the polymer liner and the metallic nozzle of the manufactured scaled-down hydrogen storage demonstrators by rotomolding process, was evaluated. The efficiency of the applied treatment on the direct adhesion of the Metal-Polymer was investigated by apparent shear test. Moreover, the microstructure of the treated interfaces was observed. Finally, the mechanical behaviors of the Metal-Polymer interface of the manufactured scaled-down storage demonstrators by rotomolding process were studied.

2.1. Materials

The manufactured scaled-down hydrogen storage tank demonstrators by rotomolding process were consisted of the polymer body (liner component) and the metallic nozzles. The liner was made of Medium Density Polyethylene (MDPE) that has a density of 0.93 g/cm^3, supplied by Matrix polymer® located in England. The metallic nozzles were made of aluminum (6061-T6) rods (Fig. 3). Following the machining process, the required nozzles (height, external radius, and inner radius of 70, 14, and 6 mm, respectively) were manufactured.

2.2. Description of the surface treatments on the metallic nozzles

2.2.1. Sandblasting treatment
Sandblasting treatment was performed with OTMT machine, model OT10 (Fig. 4). The aluminum nozzles were situated in OTMT machine and were sandblasted by SiO$_2$ particles. The efficiency of the two important parameters of the sandblasting treatment on the direct adhesion of the Metal-Polymer in the manufactured scaled-down hydrogen storage tank demonstrator by rotomolding process was investigated. The two selected parameters concerning the sandblasting treatment were the average size of the utilized SiO$_2$ particles and the blasting time/duration of the treatment. The two different considered average particle size values were 212 ± 30 and 400 ± 30 μm as the finer and coarser particles, respectively. Moreover, the different sandblasting treatment durations were 5 and 15 s. The sandblasting treatment was carried out with an air pressure of 7 bars, a blasting angle of 45°, and a blasting distance of 5 cm.

2.2.2. Flame treatment
The flame treatment efficiency on the direct adhesion of Metal-Polymer was investigated utilizing a Butane gas flame at a temperature of approximately 1000 °C. Indeed, the impact of the flame treatment was evaluated by considering the two different durations which were 5 and 60 s. Flame treatment (Fig. 5) was conducted approximately 5 cm from the top of the main reaction zone to the prepared metallic nozzles' free surfaces. Flame treatment was performed at a constant rate of 14 mm/s.

2.3. Surface topography observations

In order to obtain topographical information about surfaces, a contact profilometer (VEECO), Atomic Force Microscopes (AFM) (VEECO), Optical Microscope (OM) (ZEISS), and Scanning Electron Microscopy (SEM) (HITACHI 4800) were utilized. Indeed, the VEECO, Multi-mode Atomic Force Microscope, which was control by Nano Scope V, Silicon Nitride Tip with the constant Force of 0.12 N/m in contact mode, with the resolution of 256 was utilized to determine the roughness surface of the aluminum nozzles resulting from the flame treatment. Moreover, the Veeco profilometer with a stylus made of diamond and a radius of 12.5 μm was employed to determine the surface roughness of the sandblasted aluminum nozzles. A minimum of 10 scans were carried out for each sample. The Scanning Electron and Optical microscopes were utilized to analyze the morphology of the failure surfaces after the conducted
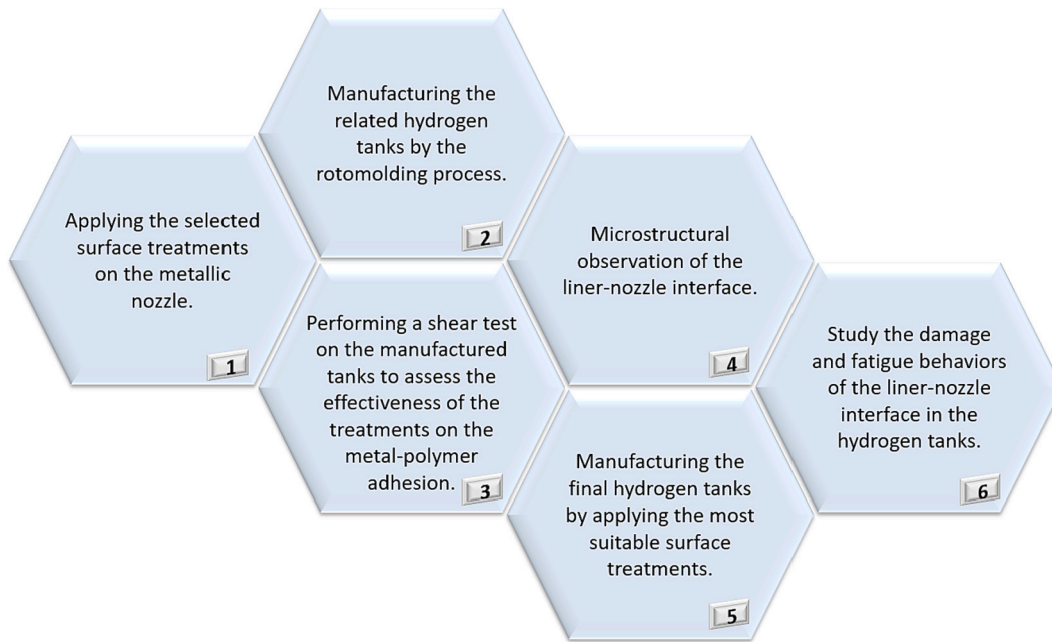
Fig. 2. The outline of the performed sequences in this study.

1. Applying the selected surface treatments on the metallic nozzle.

2. Manufacturing the related hydrogen tanks by the rotomolding process.

3. Performing a shear test on the manufactured tanks to assess the effectiveness of the treatments on the metal-polymer adhesion.

4. Microstructural observation of the liner-nozzle interface.

5. Manufacturing the final hydrogen tanks by applying the most suitable surface treatments.

6. Study the damage and fatigue behaviors of the liner-nozzle interface in the hydrogen tanks.

Aluminum rods

Machining process of Aluminum rods

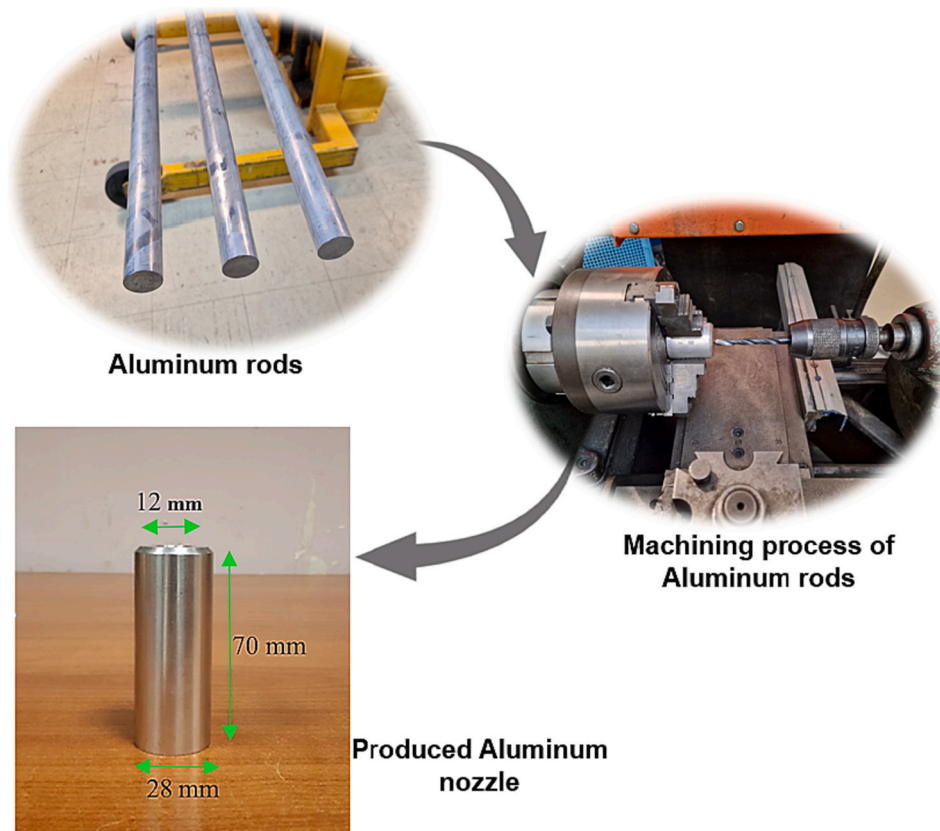Produced Aluminum nozzle

12 mm

70 mm

28 mm

Fig. 3. Process steps for manufacturing the metallic nozzles.

mechanical characterizations. Moreover, the ZEISS Optical Microscope was utilized to analyze the Metal-Polymer interlocking.

2.4. Differential Scanning Calorimetric (DSC)

An instrument of the type "TA Instruments Q10 V9.0 Build 275" was employed to determine the crystallization (T_c) and melting temperature (T_m) values of the utilized MDPE polymer. The DSC characterization was performed in the temperature range of 25 °C to 180 °C with the heating and cooling rate of 2 °C/min. The obtained melting and crystallization temperature values were 125.5 °C and 123.3 °C, respectively.
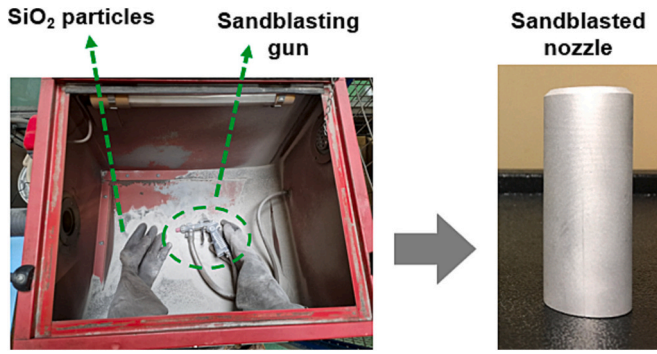
Fig. 4. Sandblasting treatment.

2.5. Rotational molding process

Scaled-down hydrogen storage tank demonstrators (samples) were manufactured by Shuttle Type Rotomoulding Machine; manufactured by STP. The in-situ temperature evolution concerning the oven, the external wall of the mold, and also the intern air during the rotational molding process was conducted utilizing the Datapaq® Tracker Telemetry system. The major and minor rotation speeds of the mold in both the heating and cooling stages of the manufacturing process were 9 and 7.5 RPM, respectively (Fig. 6).

The Datapaq® Tracker Telemetry system has enabled the depiction of the temperature changes and physical state transformations in MDPE polymer during various stages of the rotomolding process, as illustrated in Fig. 7. This information is crucial in understanding the behavior of the polymer during the rotomolding process. The point A on this diagram represents the melting of the primary powders/grains due to owning the contact with the inner surface of the mold. In the interval of A and B, the polymer grains will be melted and form successive molten layers continually. Indeed, between the A and B points, the coalescence between the solid grains occurs, continuously. This densification phenomenon will consolidate the formed part on the inner surface of the mold. The A-C interval refers to the heating stage in the rotomolding manufacturing process. Point C, is the commencement point of the cooling stage concerning the rotomolding process. The polymer material remains in a molten state until reaching the crystallization point (point D). Upon reaching point E, the material is solidified completely and the part is manufactured consequently.

Fig. 8 depicts the structure of the representative scaled-down tank demonstrator manufactured for this study. The design was based on the "value analysis" method under the ASTM - 1699-95 VE standard. This method is composed of two main phases. The external features analysis phase aims to define all the features/characteristics and requirements of the product. The second phase which is concerned the internal

functional analysis, aims to identify the technical solutions. The function and the features are listed in Table 1. Concerning the solutions, we designed a scaled-down tank demonstrator with computer tools and we submitted it to mechanical tests in order to validate the design. As is illustrated in Fig. 8, the polymer section of the manufactured scaled-down storage demonstrator is in direct contact with the half of the metallic nozzle height (35 mm).

2.6. Mechanical characterizations

The objective of the performed mechanical experiments was to evaluate the impact of the performed surface treatments utilized on the aluminum nozzles and subsequently the strength of the Metal-Polymer interface section of the manufactured specimens. The design of the utilized test specimens (scaled-down hydrogen storage tank demonstrators) was based on the "value analysis" method. For this purpose, the innovative grips and fixtures were designed that enabled us to perform the mechanical tests without the polymer liner movement during the force imposing. Indeed, the polymer liner was kept constant during the mechanical test by the designed upper and bottom plates while the nozzle was extracted by applying the force. Thus, the mode of the executed force was apparent shear on the Metal-Polymer interface (Fig. 9). This design enabled us to investigate the direct adhesion of the Metal-Polymer, which occurred during the rotomolding process.

The apparent shear test was conducted using the INSTRON 5881 tensile machine at a strain rate of 2 mm/min at room temperature. Moreover, the stress-controlled fatigue test was performed utilizing the MTS 830 hydraulic Machine in 1 Hz as frequency and $R = \sigma_{min} / \sigma_{max} = 0.1$.

2.7. Validation of the mechanical characterization approach

To evaluate the proposed method for mechanical testing and characterization, we used 3D finite element analysis. Our overall objective was to evaluate the bond strength at the interface between metal and polymer components within a scaled-down hydrogen storage tank demonstrator under static conditions. It's important to emphasize that the objective of the finite element calculation presented focuses on a qualitative analysis of the stress profile at the metal-polymer interface in order to validate the test method by verifying that there is no local stress concentration.

The penalty method was utilized to model the surface interactions and determine the stress distribution. Our finite element model was built in Abaqus, replicating the same geometry and material properties as our physical experiments. The demonstrator tank was discretized using the SOLID185 linear finite element software. To ensure computational stability, we selected 3D element types for deformation, stress and strain analysis.

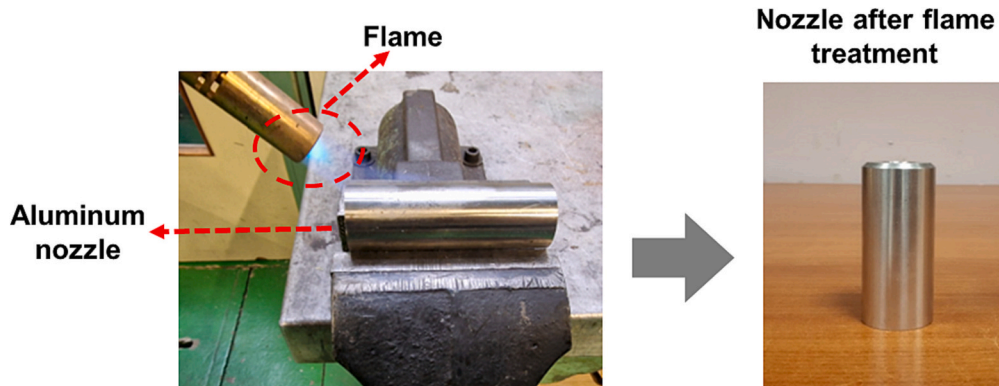Fig. 10 clearly illustrates the uniform stress distribution during the
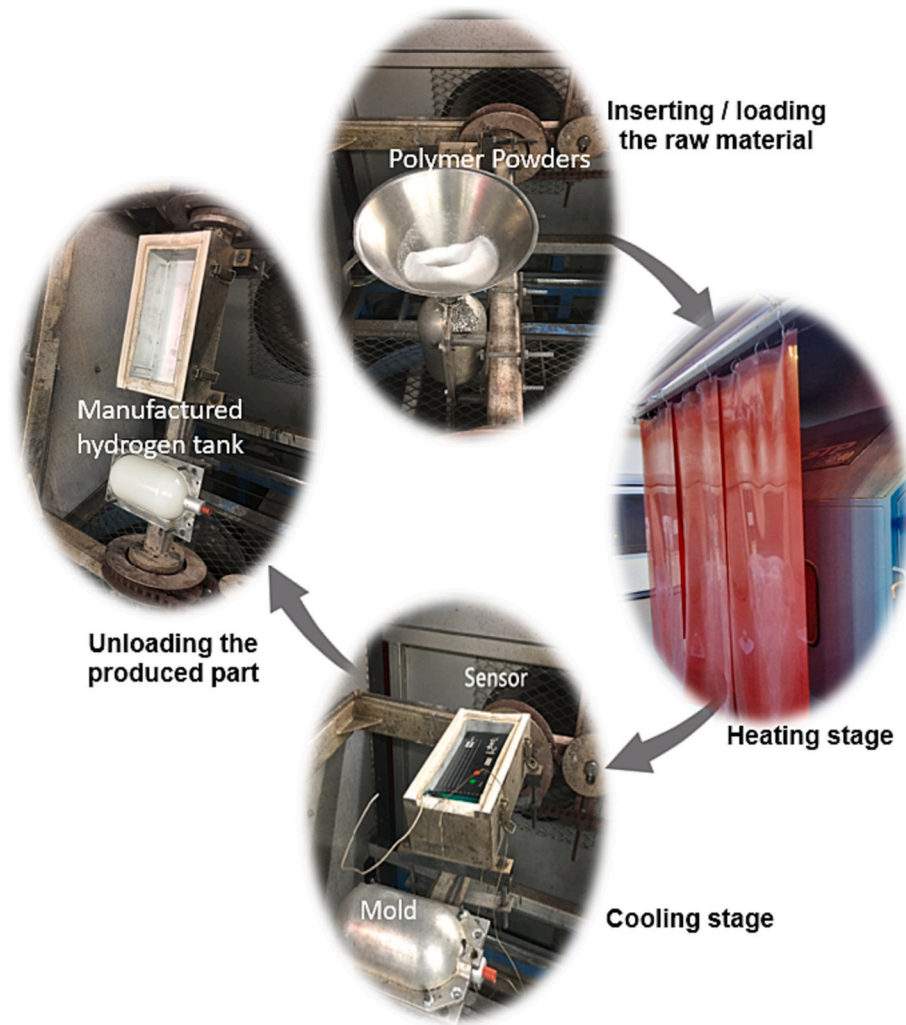

Fig. 5. Flame treatment.

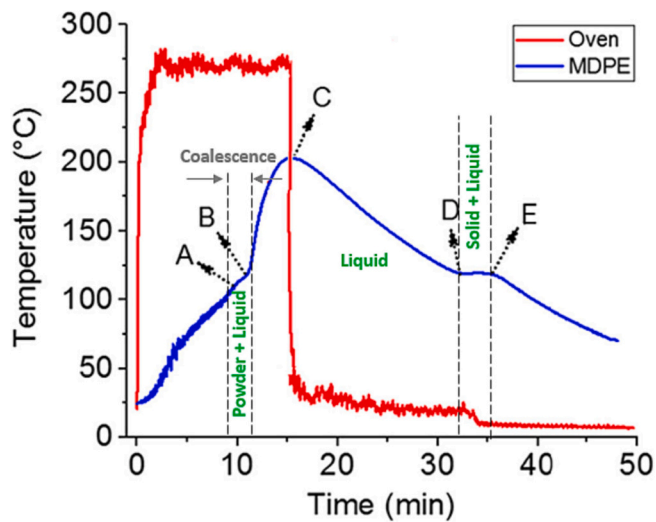5

Fig. 6. Rotational molding process.

Fig. 7. Temperature evolution of polymer and oven during rotational molding process [30].

shear test performed on the metal-polymer interface, confirming the location of the critical region in this interface when applying our designed mechanical characterization approach. Furthermore, this figure validates the uniform shear stress distribution at the metal-polymer interface, confirming the efficacy of our mechanical testing approach as a representative method for assessing the shear strength in our scaled-down hydrogen storage tank demonstrators, which aim to mimic the boss-liner bond in actual hydrogen storage tanks.

3. Results and discussions

3.1. Sandblasting surface treatment

An investigation was conducted to determine how sandblasting treatment affected the adhesion between Al and MDPE. Indeed, an assessment of the influence of some related parameters was conducted on Al-MDPE adhesion. As was stated the studied parameters were the average size of the utilized SiO_2 particles (mesh) and also the blasting time (duration).

3.1.1. Effect of blasting duration

In order to study the influence of blasting duration on Metal-Polymer adhesion, sandblasting was conducted using two different SiO_2 particle sizes (the finer and coarser meshes) and two different blasting durations. As was stated the two different selected process durations were 5 and 15 s. In the first step, two samples (Aluminum, 6061-T6 rods as metallic nozzles) were sandblasted for 5 and 15 s with the finer mesh, followed by the manufacturing of the scaled-down reservoir demonstrators and the subsequent apparent shear test. Indeed, the average apparent shear
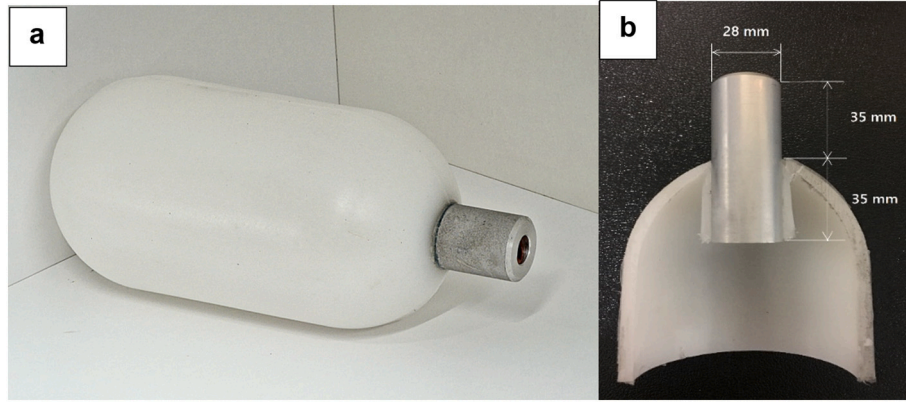
Fig. 8. (a): The manufactured scaled-down hydrogen storage tank demonstrators; (b): Cross-section viewpoint of manufactured sample.
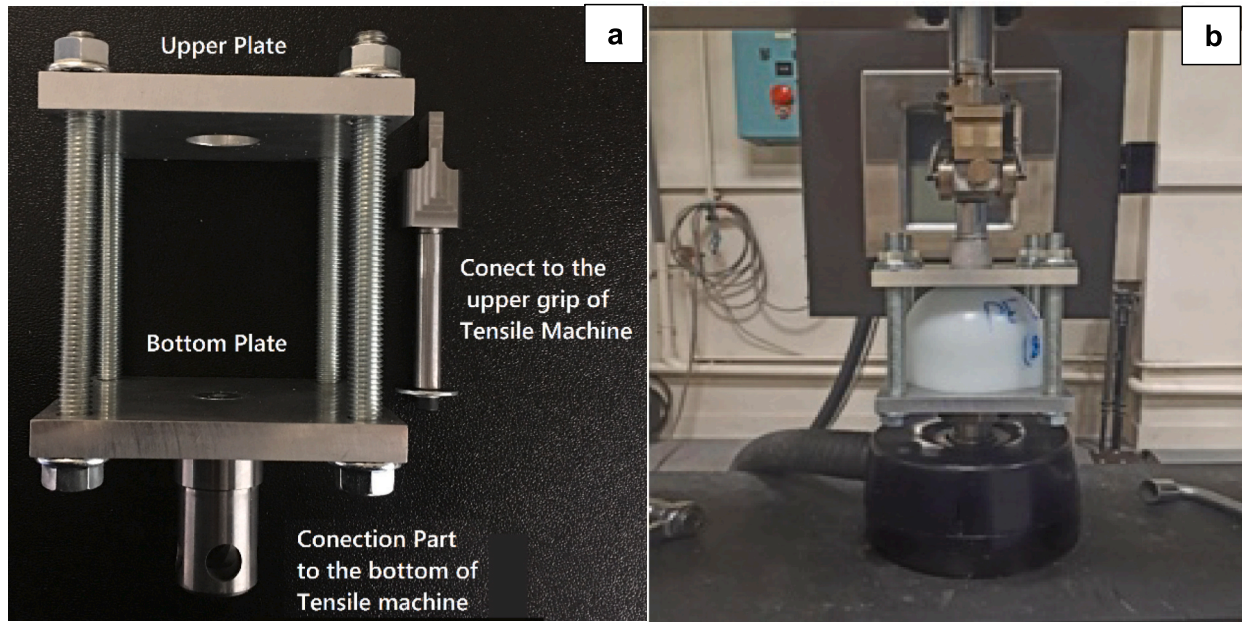

Fig. 9. The designed mold for mechanical test (a), performing the mechanical characterizations (b).

stress applied on the Al (6061-T6)-MDPE interface. The obtained average apparent normalized shear strength values were 4.57 ± 0.08 MPa and 5.13 ± 0.05 MPa concerning 5 s and 15 s sandblasted samples, respectively.

The surface roughness of Al rods after the blasting durations of 5 s and 15 s using the finer meshes was evaluated with the profilometer. The obtained R_a (Arithmetic Roughness) values were 4.9 μm and 5 μm corresponding to the blasting durations of 5 and 15 s, respectively (Fig. 11).

According to the obtained results from the conducted apparent shear test, the blasting process utilizing the finer meshes could enhance the Metal-Polymer adhesion through the rotomolding process, compared to the non-treated specimens. While the duration of the sandblasting process didn't have any significant effect on the Metal-Polymer interface strength (Fig. 12, left). Also, increasing the sandblasting process duration, didn't influence the modulus. Moreover, the optical microscopy observations illustrated that the sandblasting process by the finer mesh could develop the roughness and asperities, and subsequently the mechanical interlocking of the metal and the polymer during the rotomolding process. While, the provided surficial asperities on the metal substrate during 5 and 15 s, have kind of same size and geometries (Fig. 12, right).

Moreover, the sandblasting process also was performed by the coarser meshes during 5 and 15 s as the different process durations on the surface of the Al rods as metallic nozzles of the scaled-down reservoir demonstrators. Then, profilometer measurements were conducted on Al rods after blasting durations of 5 and 15 s. Based on the blasting durations of 5 s and 15 s, R_a (Arithmetic Roughness) values of 6 μm and 9 μm were obtained, respectively (Fig. 13).

Finally, the related scaled-down reservoir demonstrators were manufactured by rotomolding process and consequently were tested. The obtained average apparent normalized strength concerning the process durations of 5 and 15 s were 5.1 ± 0.03 MPa and 6 ± 0.04 MPa, respectively (Fig. 14, left). According to the apparent shear test results regarding the utilization of the coarser meshes, by increasing the sandblasting process duration (by the coarser meshes), the adhesion and interface strength of the Metal-Polymer was increased. Indeed, the profilometry results illustrated that an increase in sandblasting duration led to an increase in Al substrate surficial roughness and mechanical interlocking of Metal-Polymer, consequently. Based on the apparent shear test results, the blasting process utilizing the coarser meshes improved the Metal-Polymer adhesion during rotomolding as compared to non-treated samples. Moreover, regarding the utilization of the coarser meshes, by increasing the sandblasting process duration (by the coarser meshes) from 5 s to 15 s, the adhesion and interface strength of
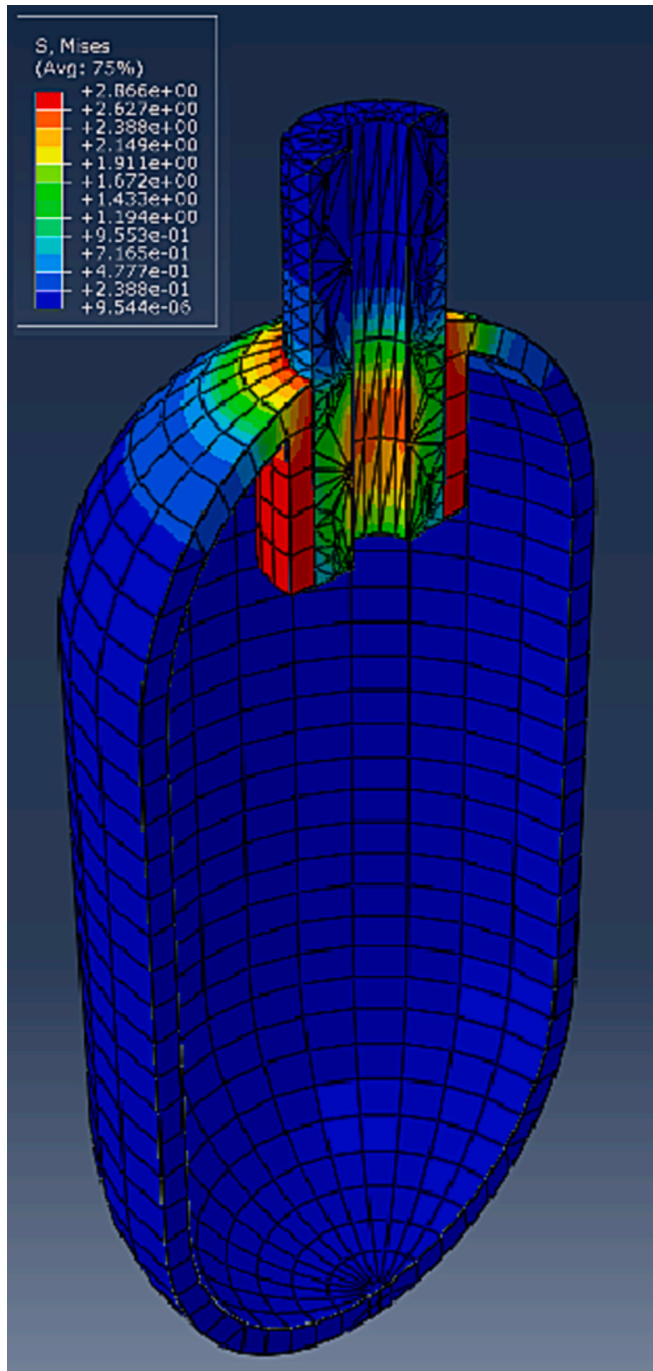
Fig. 10. Stress distribution concerning the friction coefficient of 1 (perfect adhesion).
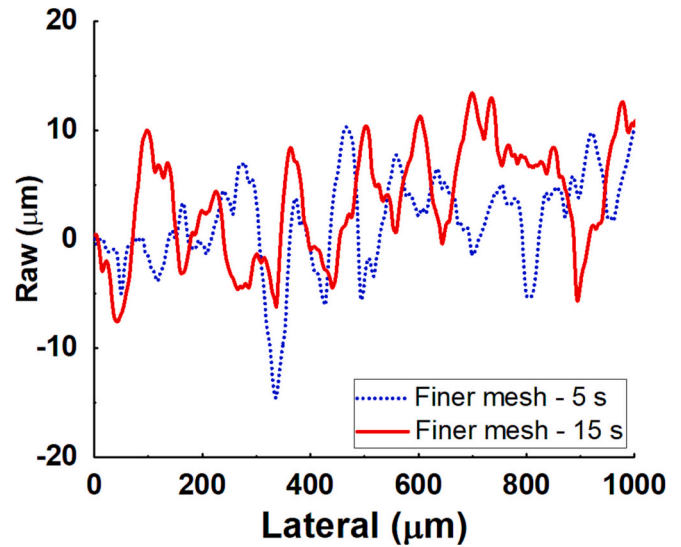

Fig. 11. The obtained Profilometry curves concerning the developed surficial asperities from the 5 and 15 s sandblasting process utilizing the finer meshes.

the sand blasting duration with the utilization of the coarser particles. As the duration of the related particles increased, the depth of the surficial asperities is developed, too. This caused the increase of the free surface of the substrate and subsequent development of the mechanical interlocking and the friction of the Metal-Polymer.

3.1.2. Effect of SiO₂ particle size (mesh)

As was explained, two different SiO_2 particle sizes (meshes) were utilized for sandblasting treatment. The different particle sizes were 212 μm and 400 μm as finer and coarser meshes, respectively. No significant difference was observed in the obtained Metal-Polymer interface strength after 5 s of sandblasting with finer or coarser particles (Fig. 15a).

Fig. 15b illustrates the results obtained regarding the utilization of coarser and finer particles during 15 s sandblasting process. As a result of employing coarser SiO_2 particles during the 15-second sandblasting process, more strength could be achieved in the Metal-Polymer interface than with finer SiO_2 particles. This increase in the strength was more tangible comparing the utilization of the coarser SiO_2 particles during the 5-second sandblasting process. Moreover, the implementation of coarser SiO_2 particles during the 15-second sandblasting process exhibited increased elongation at break, leading to more failure ductility. In general, it was determined that this treatment has a favorable impact on boosting the strength of the Metal-Polymer interface based on the outcomes of the apparent shear test and microscopic observations connected to the sandblasting of the surface of aluminum 6061-6 T employing SiO_2 particles. Additionally, the two related variables under consideration—namely, the sandblasting time and the size of the SiO_2 particles—have an effect on the efficiency of the sandblasting treatment in the issue of the Metal-Polymer interface adhesion with regard to the scaled-down hydrogen storage tank demonstrators produced using rotational molding process. Indeed, the effect of the SiO_2 particle size was noticeable in case of the longer considered period of sandblasting treatment. Furthermore, the effect of the sandblasting duration was more evident in case of the coarser SiO_2 particles utilization.

3.2. Metal surficial flame treatment

Flame was considered as a surface treatment for the metal. So that, the Aluminum, 6061-T6 rods as the metallic nozzles of the scaled-down hydrogen storage tank demonstrators were exposed to flame. It was
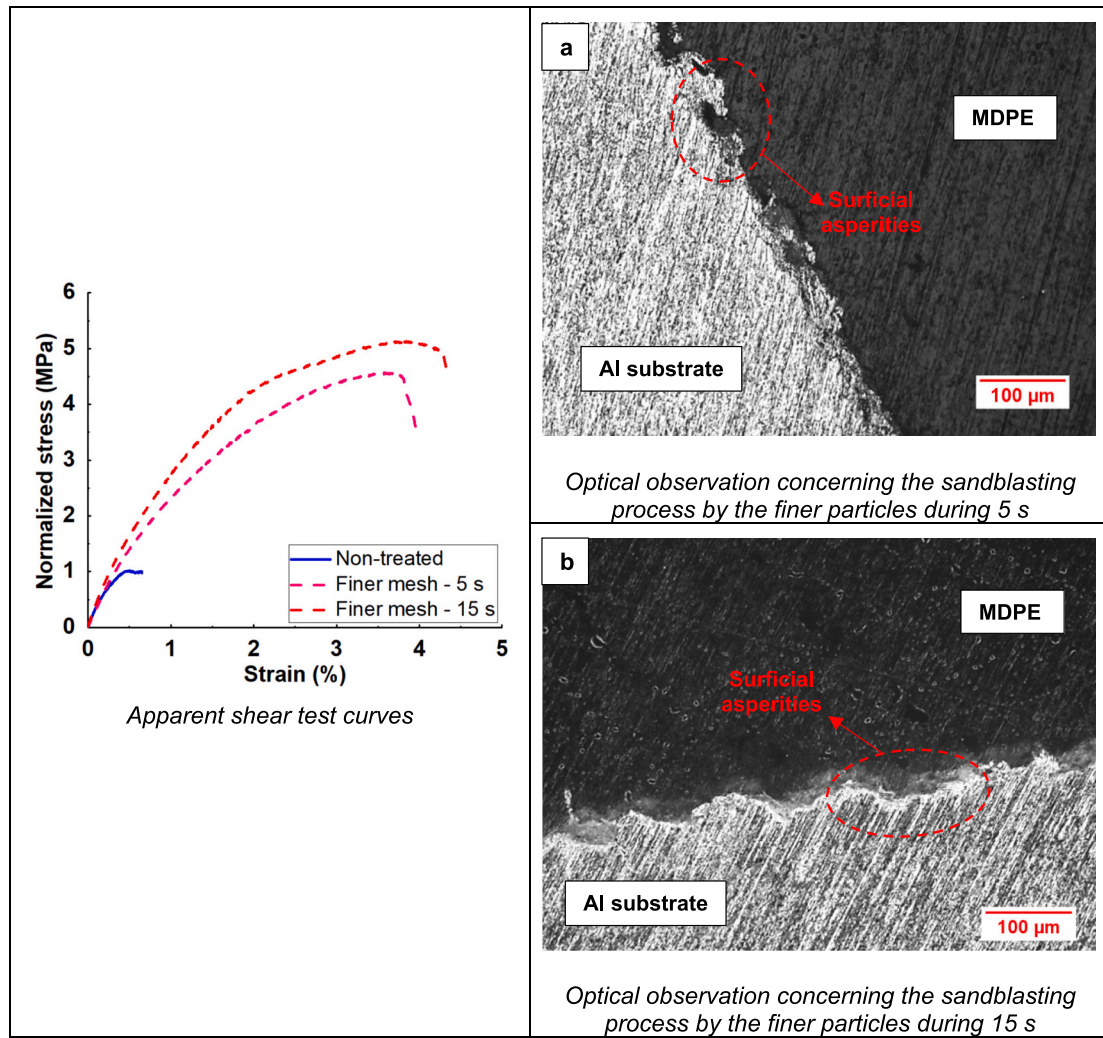
the Metal-Polymer increased more sensible comparing the finer mesh utilization. The outcomes of the profilometry analysis indicate that an increase in sandblasting duration correlates with a corresponding escalation in the Al substrate's surficial roughness and the mechanical interlocking of Metal-Polymer. These findings suggest that extending the sandblasting period can enhance the adhesion properties of the Metal-Polymer interface. While the duration of the sand blasting process didn't have any significant effect on the enhancement of the modulus of the Metal-Polymer interface. The surficial microstructure of the Al substrates sandblasted by the coarser particles was observed by the optical microscope (Fig. 14, right). It was observed that the coarser particle could provide the considerable asperities on the surface of the Al substrate during the sand blasting process. Fig. 14 depicts the effect of

Fig. 12. Apparent shear curves of the non-treated and sandblasted samples with the finer SiO_2 particles during 5 and 15 s (left) and the optical observations of mechanical interlocking in the Metal-Polymer interface (right).
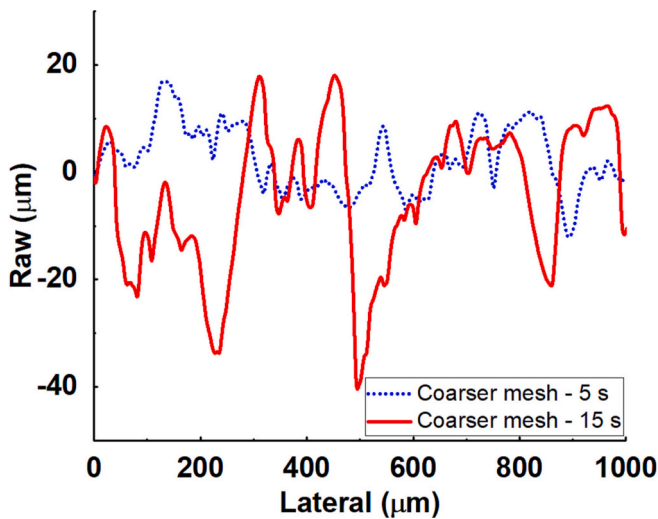

Fig. 13. The obtained Profilometry curves concerning the developed surficial asperities from the 5 and 15 s sandblasting process utilizing the coarser meshes.

decided to cut some pieces of these metallic nozzles (metallic morsels) in order to determine the effect of the flame on the surficial Al rods. Hence the surface of the prepared metallic morsels (5×5 mm^2) was exposed to the flame treatment in the two different durations of the 5 and 60 s. Then, the surface of the Al morsels was observed under optical microscope (Fig. 16). Fig. 16 depicts the cross-section views of the non-flamed and the flamed Al morsel during 60 s. The related microscopy observations illustrated that the flame treatment caused surficial asperities, which may contribute to the mechanical interlocking of the polymer and metal agents and the subsequent Metal-Polymer interface strength.

As the results of AFM characterization, the surficial roughness of the non-flamed (non-treated) Al nozzles and the flamed Al morsels were 65.9 nm and 98.3 nm, respectively (Fig. 17). Indeed, the flame treatment caused the local melting of the Al surface and formation of the oxide layers. Flame treatment was therefore considered for more studies as the promising treatment in order to increase the Metal-Polymer interface strength.

According to the results of topography and microscopy analysis (Figs. 16 and 17) of the non-treated Al rods (as-machined), the utilized machining procedure as the initial step in the fabrication of the aluminum rods resulted in the asperities on the surface of the rods. Therefore, prior to flame treatment, sandblasting was considered as a means of achieving similar and homogenous roughness on the surfaces of the Al rods to avoid the intervention of the machining history and concentrate the study just on the flame treatment impact. Hence,
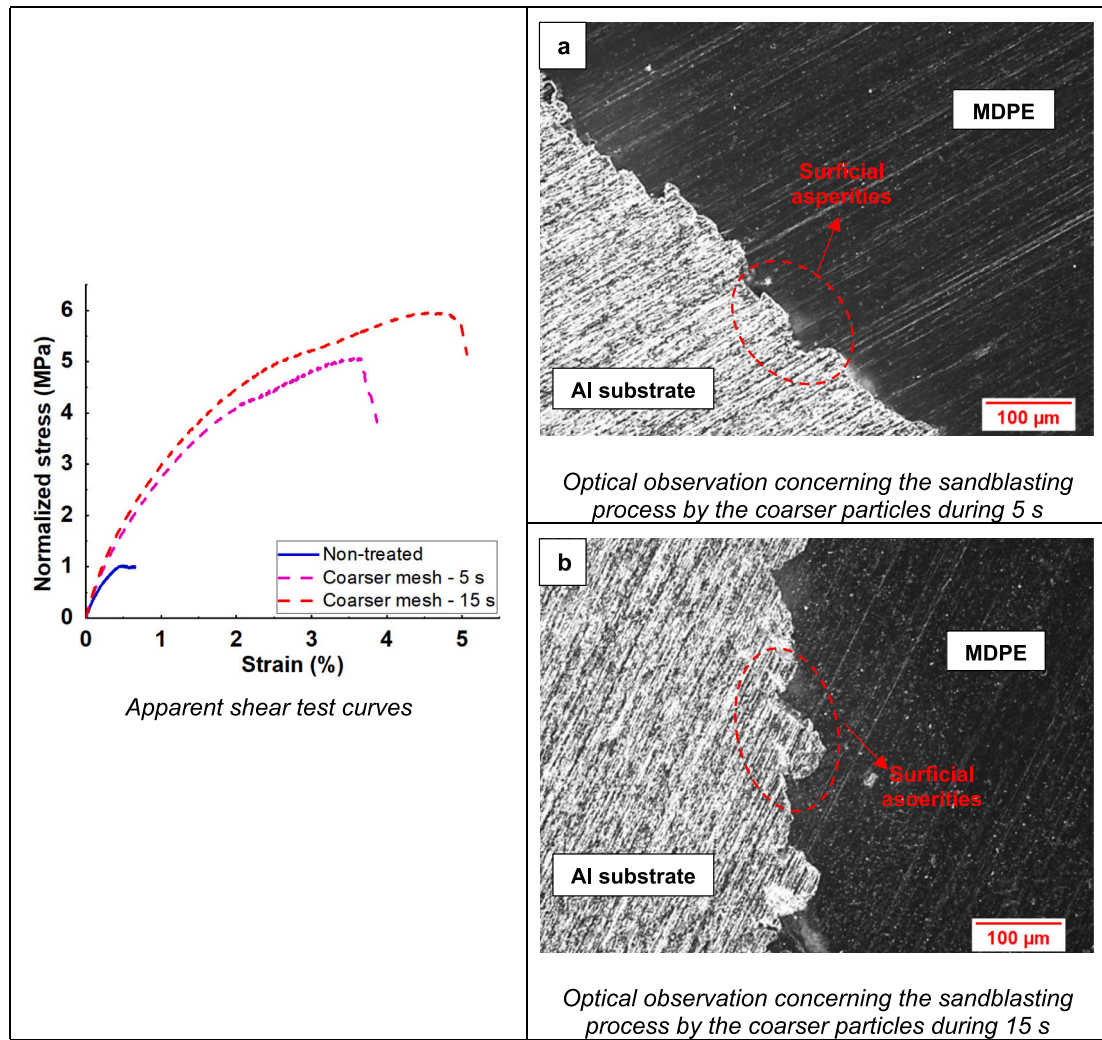
Fig. 14. Apparent shear curves of the non-treated and sandblasted samples with the coarser SiO$_2$ particles during 5 and 15 s (left) and the microscopy observations of mechanical interlocking in the Metal-Polymer interface (right).
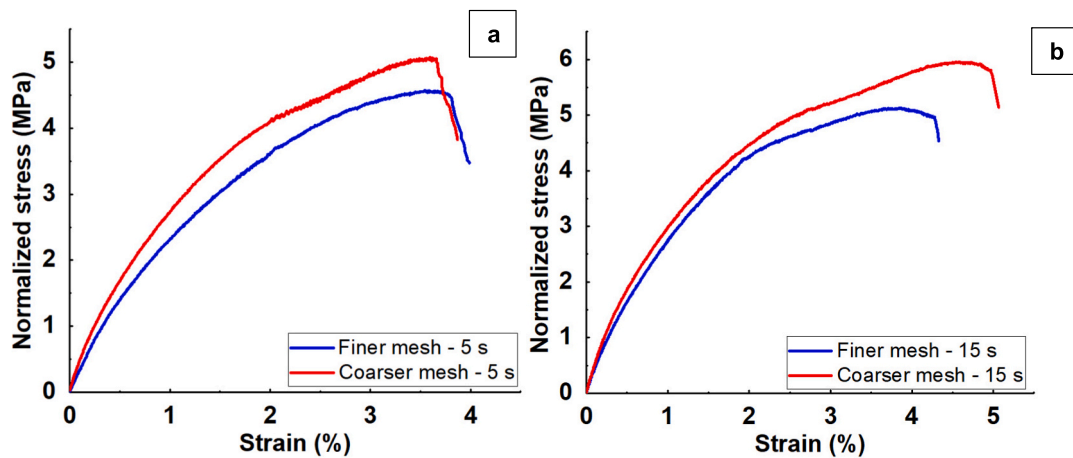

Fig. 15. Apparent shear curves of the sandblasted samples with the coarser and finer SiO$_2$ particles during 5 s (a) and 15 s (b).

sandblasting with the coarser particles for 15 s (which exhibited superior efficiency on the Metal-Polymer adhesion) was applied.

In order to obtain an accurate appraisal of the effectiveness of the flame process in strengthening the Metal-Polymer interface on scaled-down hydrogen storage tank demonstrators manufactured by the rotational molding, two different treatment durations were selected. The flaming treatment of 5 and 60 s was decided for application on Al nozzles following sandblasting. Consequently, the Al nozzles were flame-exposed for 5 and 60 s after being sandblasted by the coarser particles for 15 s. Following the treatment of the Al nozzles, the scaled-
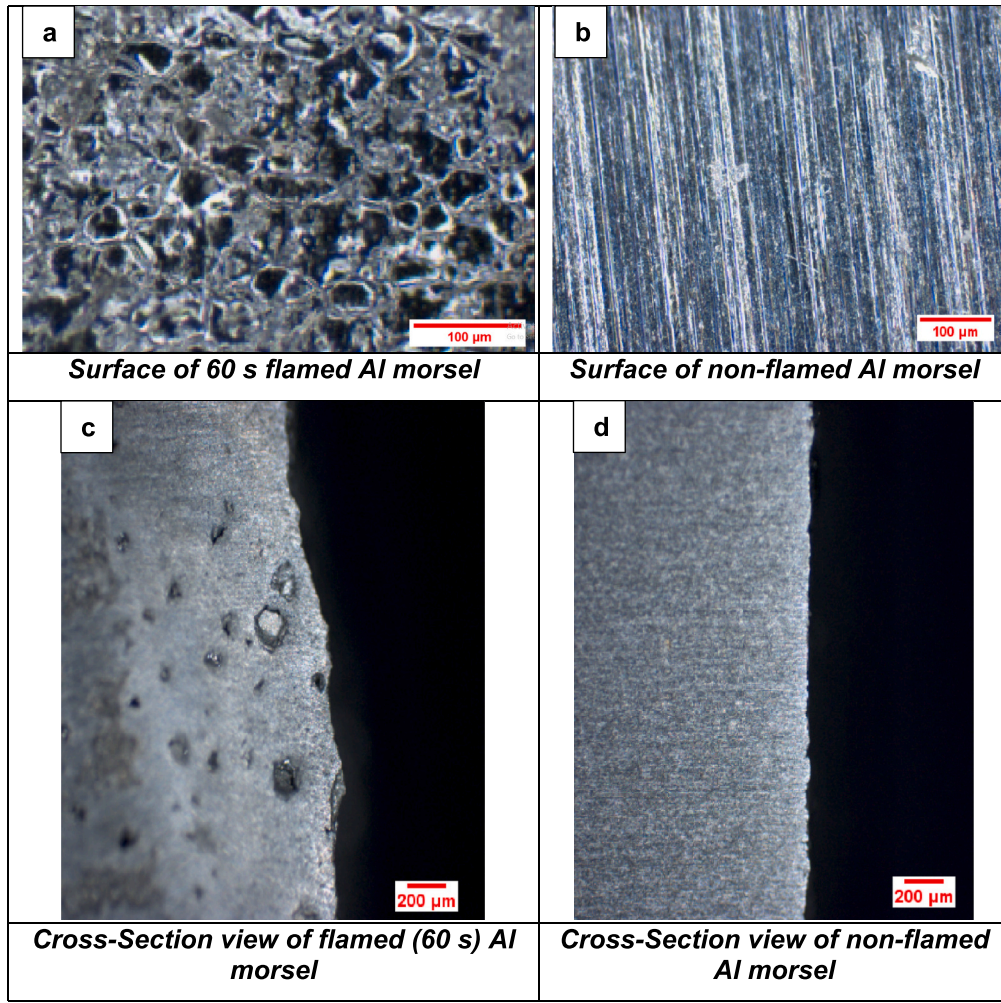
Fig. 16. Microscopy observations of the flamed and non-flamed Al morsels.

down hydrogen storage tank demonstrators were manufactured using rotational molding and apparent shear tests were conducted on the scaled-down hydrogen storage tank demonstrators (Fig. 18).

Fig. 18 depicts the effect of the flame treatment duration, on the improvement of the Metal-Polymer interface strength. It is illustrated that the selected flame durations could not have a substantial impact on the Metal-Polymer adhesion. In general, comparing the obtained sandblasting and flame treatments results, the flame treatment couldn't provide a significant and efficient impact on the Metal-Polymer adhesion.

3.3. Damage analysis

In the course of determining the most effective treatment on the metallic nozzles to achieve a stronger adhesion between our choices, it was illustrated that sandblasting with the coarser particles during 15 s produced the most beneficial outcome. Therefore, after designing the scaled-down hydrogen storage tank demonstrators, their damage behavior was studied. Stiffness reduction is an appropriate macroscopic damage indicator to define damage development in short fiber reinforced composite materials. In the case of apparent shear loading, one can define a macroscopic damage variable as:

$$D_{macro} = 1 - C_D/C_0$$

whereas C_0 and C_D are the modulus of virgin and damaged structure, respectively. Fig. 19 depicts the possible joining mechanisms in Metal-Polymer hybrids.

An experimental stress-strain curve for quasi-static loading-unloading apparent shear test concerning the sandblasted (coarser mesh – 15 s) scaled-down storage demonstrators is shown in Fig. 20. Fig. 21 illustrates the evolution of the macroscopic damage parameter of these scaled-down storage demonstrators, D, under quasi-static loading-unloading apparent shear test as a function of applied stress. It should be indicated that, several tests (at least 3) were performed and the results have been reported in this figure in such a way that at least 6 points have been measured until the very last stages just before failure. One can note that the value of macroscopic damage parameter remains very low until about apparent stress of 0.6 MPa. This confirms that interface failure remains limited. After this value the macroscopic damage is clearly observed which corresponds to first non-linearity of apparent stress-strain curve in monotone loading.

3.4. Fatigue behavior

Fig. 22, depicts the Wohler curves obtained in apparent shear-shear stress-controlled fatigue tests at the frequency of 1 Hz for the manufactured scaled-down hydrogen storage tank demonstrators concerning the non-treatment and sandblast treatment utilizing coarser mesh during 15 s. Indeed, the fatigue test was performed in the different constant levels of stress. The Wöhler curves obtained from fatigue tests conducted on non-treated and sandblasted (coarser mesh - 15 s) scaled-down storage demonstrators at 1 Hz revealed a linear fatigue behavior. This finding indicates that the specimens under investigation exhibit a consistent reduction in strength under cyclic loading. The observed
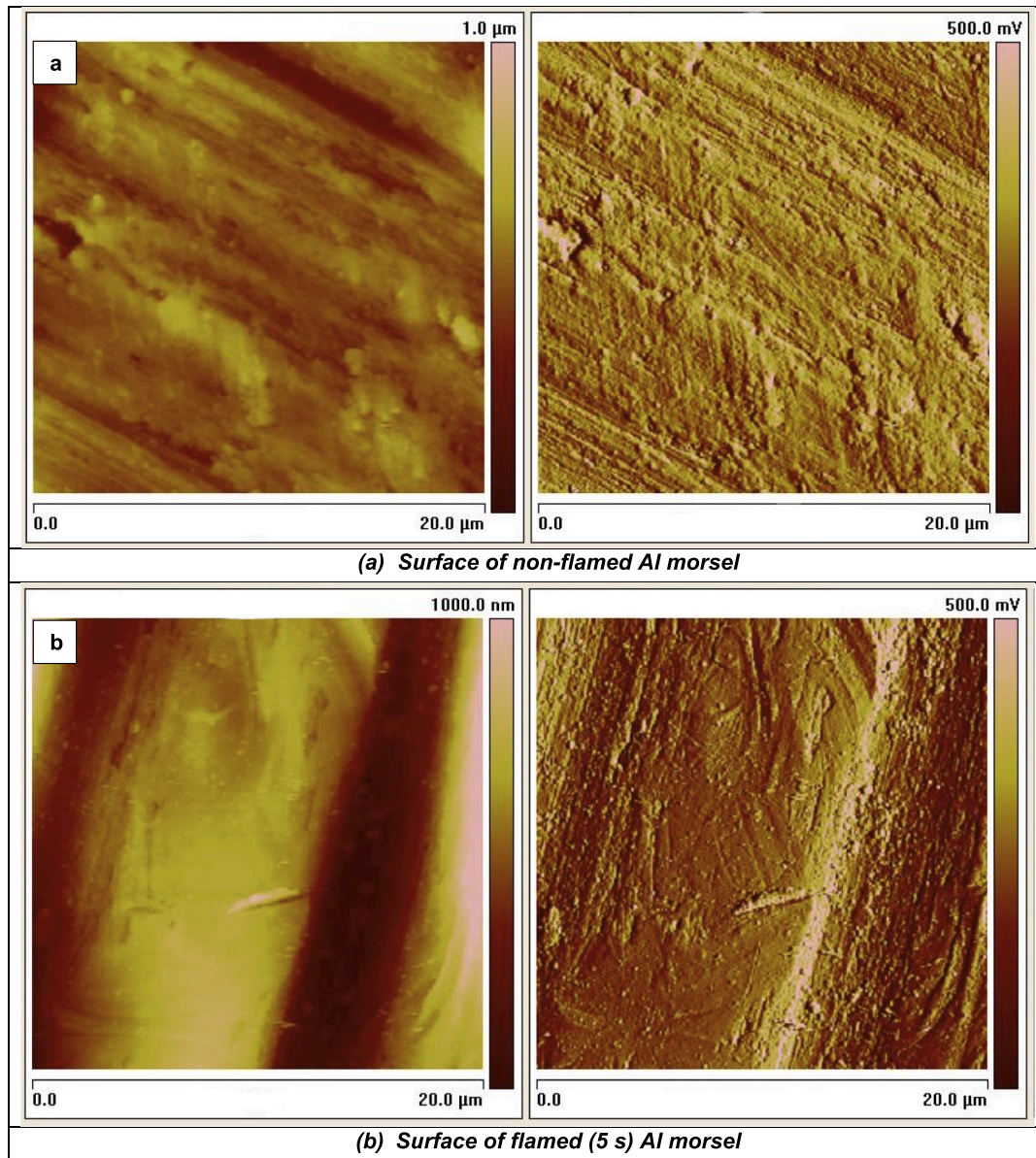
(a) Surface of non-flamed Al morsel

(b) Surface of flamed (5 s) Al morsel

Fig. 17. AFM Topography images of the non-flamed (a) and flamed Al morsels (b).

behavior is of interest for the design and durability of the structure subject to cyclic loading. The results obtained from this study will contribute to the ongoing efforts to understand the mechanisms underlying fatigue failure and the development of strategies to mitigate its effects. Moreover, the Wöhler curves didn't displayed a clear asymptotic value representative of an endurance limit, in contrast to most of the metal materials.

It can be noticed that the non-treated and sandblasted (coarser mesh – 15 s) scaled-down storage demonstrators displayed apparent endurance strength values of 0.4 and 1.10 MPa in about 200 cycles (Low Cycle Fatigue (LCF) region), respectively. Moreover, the non-treated and sandblasted (coarser mesh – 15 s) scaled-down storage demonstrators displayed apparent endurance strength values of 0.23 and 0.65 MPa in about 10^5 cycles (High Cycle Fatigue (HCF) region). Therefore, manufactured sandblasted scaled-down storage demonstrators exhibited higher fatigue strength levels in LCF and HCF regimes in comparison with the non-treated scaled-down storage demonstrators. Consequently, the sandblasting treatment (coarser mesh – 15 s) exhibits a positive impact on the fatigue strength improvement of the direct adhesion of the

Metal-Polymer interface in the manufactured scaled-down hydrogen storage tank demonstrators by rotational molding process. Moreover, the range of the fatigue strength values concerning the studied fatigue cycles is wider in the case of the sandblasted (coarser mesh – 15 s) scaled-down storage demonstrators.

Furthermore, the drop fatigue strength amount from LCF to HCF regions in the sandblasted (coarser mesh – 15 s) scaled-down storage demonstrators was more significant compared to the non-treated scaled-down storage demonstrators. The stated drop endurance strength in sandblasted scaled-down storage demonstrators compared to the non-treated ones—due to the passing from the LCF to HCF regions—is highlighted in the slop of the related Wöhler curves (Fig. 22). Consequently, the sensitivity to the fatigue cycles is more significant in the sandblasted (coarser mesh – 15 s) scaled-down storage demonstrators. However, the percentage values concerning the fatigue strength drop from the same cycles in LCF to HCF were so close in both cases of the non-treated and sandblasted (coarser mesh – 15 s) scaled-down storage demonstrators. Indeed, the fatigue strength of the non-treated and sandblasted (coarser mesh – 15 s) scaled-down storage demonstrators
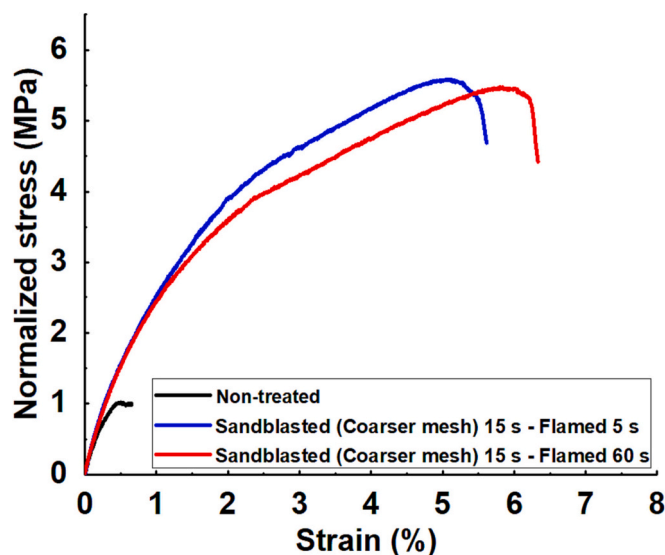
Fig. 18. Apparent shear curves of the flamed samples in the different durations.

Fig. 20. Damage mechanisms under quasi-static loading unloading apparent shear test concerning the manufactured scaled-down hydrogen storage tank demonstrators after the sandblasting treatment utilizing coarser mesh during 15 s.
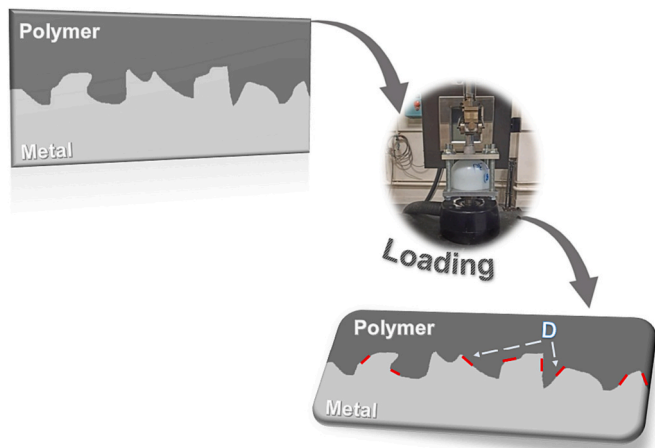

Fig. 19. Possible joining mechanisms in Metal-Polymer-Hybrids.

from 200 cycles to 10^5 cycles led to drop percentages of about 42 % and 40 %, respectively. Therefore, the sandblasting effectively increased the fatigue performance of the Metal-Polymer interface.

3.4.1. Relative modulus in fatigue

The relative modulus is generally identified to be an efficient parameter to detect the presence and evolution of damage during cyclic loading. It can also be used in a stiffness-based fatigue failure criterion. The relative modulus is defined as the modulus C at each stage of the fatigue test divided by the virgin structure modulus (i.e. without previous loading and damaging history), C_0. Fig. 23 depicts the evolution of the relative modulus under the different amplitudes at 1 Hz concerning the sandblasted (coarser mesh – 15 s) scaled-down storage demonstrators.

One can note the relative stability of the modulus which appears as a long plateau until failure, independently on the applied amplitudes. No significant loss of stiffness is observed just before failure of structure whereas damage development is not progressively step which observed in Fig. 23. In the case of low amplitude (0.7 MPa) there is no macroscopic modulus reduction. Indeed, this curve illustrates that under fatigue loading, there is no macroscopic damage until the certain number of cycles according to the applied stress. Upon reaching these values, the
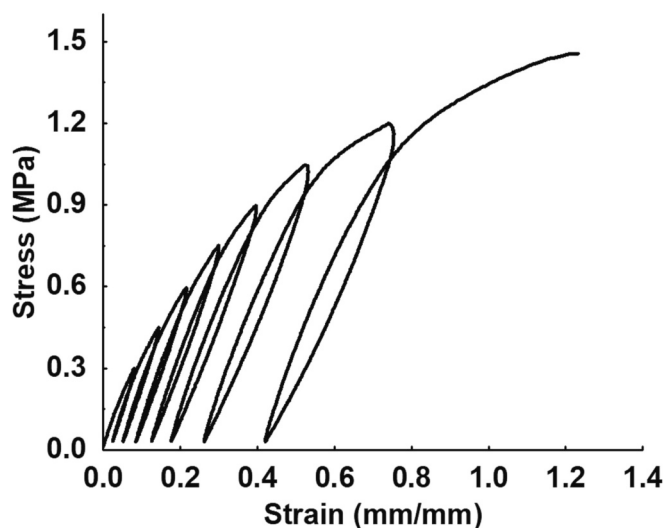
progressive damage between the metal and polymer occurs until the decohesion of two parts.

Fig. 24 illustrates the polymer residues on the sandblasted Al nozzle surface (utilizing coarser mesh during 15 s), following the fatigue test. The SEM observations indicate that the polymer residues (representing the polymer agent) are visible on the metallic substrate. However, the protruding polymer sections (circled sections) depict the failure occurrence in the surficial layers located more along the depth of the polymer agent. The protruding polymer sections were more evident after the applied fatigue test in lower amplitudes than in higher amplitudes. It illustrates that the Metal-Polymer interface of the manufactured scaled-down hydrogen storage tank demonstrators sustained less damage and fracture when lower amplitude loads were applied. This keynote can be considered throughout both the design and the service.

4. Conclusion

The primary aim of this investigation was to assess the effectiveness of various metal surface treatments in enhancing the direct adhesion of the Metal-Polymer interface within type IV hydrogen storage liners, fabricated using the rotomolding process. In pursuit of this objective, a comprehensive analysis of the damage and fatigue behavior of the metal-polymer interface was conducted using a representative demonstrator. The results revealed that the sandblasting treatment led to a significant improvement in the direct adhesion between the Metal-Polymer components. Furthermore, the efficacy of the sandblasting treatment was enhanced when coarser particles were employed and the treatment duration was extended. Conversely, the flame treatment exhibited negligible impact on the apparent shear strength of the Metal-Polymer interface. In the final phase of this study, employing the most suitable parameters derived from the investigated treatments, an exploration was conducted into the damage and fatigue life of the optimized Metal-Polymer interface. In terms of fatigue strength, the studied Metal-Polymer interface displayed an almost linear relationship with load amplitude. In contrast to metallic materials, the Wöhler curves of the examined interface did not manifest a distinct asymptotic value indicative of an endurance limit. During fatigue loading, a relative stability of the modulus was observed which exhibited a prolonged plateau until failure, regardless of applied amplitudes. Notably, there was no significant degradation in stiffness immediately prior to structural
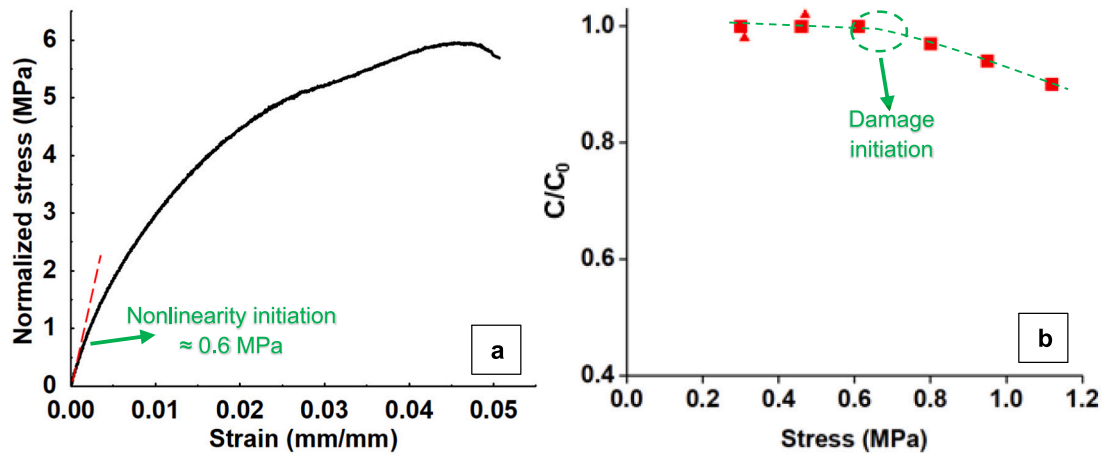
Fig. 21. Applied stress vs. macroscopic damage evolution in the manufactured scaled-down hydrogen storage tank demonstrators after the sandblasting treatment utilizing coarser mesh during 15 s.
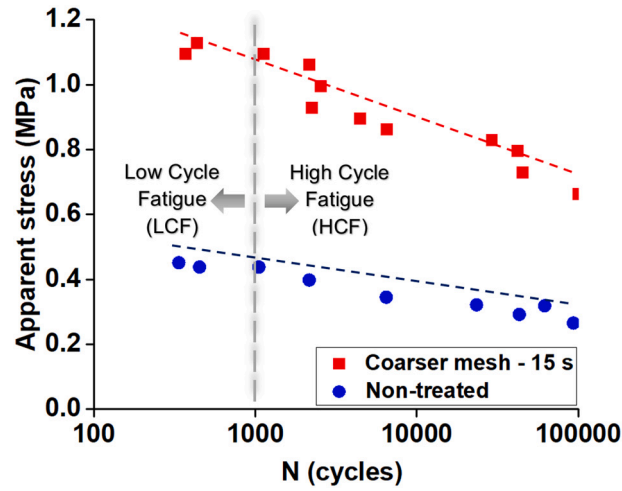

Fig. 22. Wöhler curves performed on the scaled-down hydrogen storage tank demonstrators under apparent shear-shear fatigue loading.
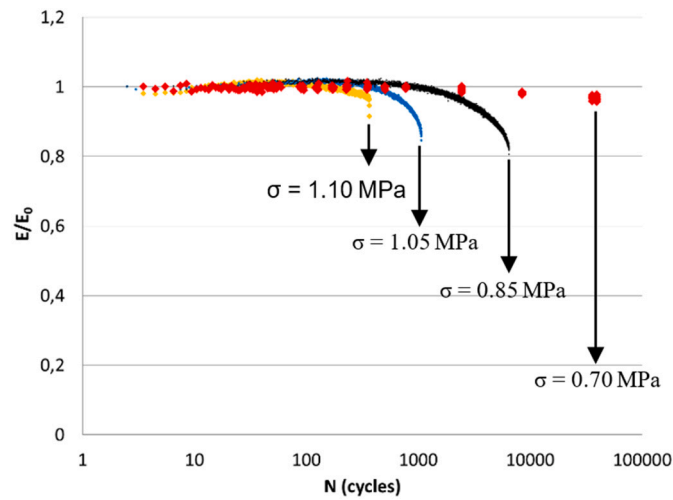

Fig. 23. Relative modulus evolution under different loading amplitudes.
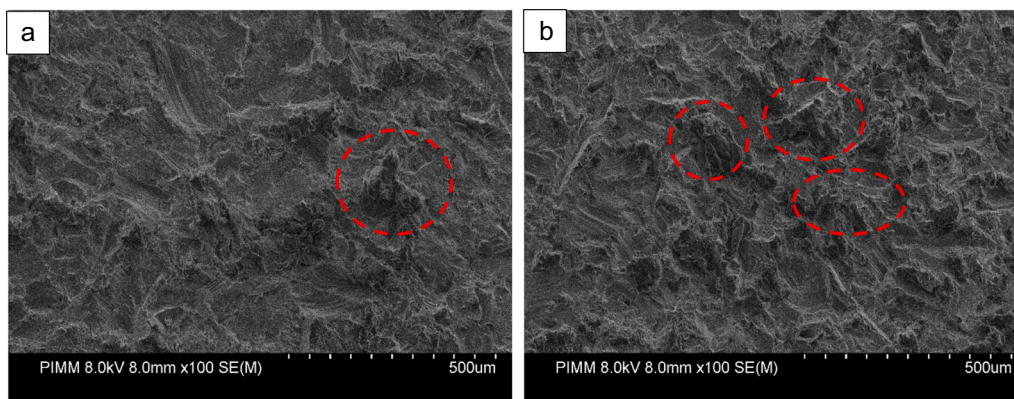
Fig. 24. SEM observations of high amplitude (a) and low amplitude (b) concerning the sandblasted (coarser mesh – 15 s) scaled-down storage demonstrators.

failure, despite the non-linear nature of damage progression.

In summary, these findings provide valuable insights into optimizing the adhesion and fatigue behavior of the boss-liner interface within the realm of hydrogen storage liner technology, aligning with the rigorous scientific context of the study.

Moving forward, there are promising paths to explore based on our study's findings. One is refining surface treatments using advanced methods and multi-scale analysis for better Metal-Polymer adhesion. Additional avenues involve delving into the optimization of long-term interface durability and simulating authentic operational conditions for enhanced hydrogen storage tanks.

CRediT authorship contribution statement

M. Ahmadifar: Supervision, Conceptualization, Methodology, Data curation; Formal analysis, Writing – original draft, review & editing., Visualization.

K. Benfriha: Supervision, Writing – review & editing., Methodology, Visualization, Methodology, and Formal analysis.

M. Shirinbayan: Writing – review & editing., Methodology, Formal analysis, and Visualization.

A. Aoussat: Writing – review & editing., Methodology.

J. Fitoussi: Supervision, Writing – review & editing., Visualization, Methodology, Data curation and Formal analysis.

Declaration of competing interest

We declare that no significant result contained in our proposal has been published formerly without citation and is not currently envisaged for publication elsewhere. No associated conflicts of interest should likewise be declared and no financial support was provided for this work, which could influence the outcomes.

Data availability

Data will be made available on request.

Acknowledgements

References

[1] Dorit Munzke, et al., Monitoring of type IV composite pressure vessels with multilayer fully integrated optical fiber based distributed strain sensing, Mater. Today: Proc. 34 (2021) 217–223.

[2] D.J. Durbin, Cecile Malardier-Jugroot, Review of hydrogen storage techniques for on board vehicle applications, Int. J. Hydrog. Energy 38 (34) (2013) 14595–14617.

[3] Xiulei Wang, et al., Advances on materials design and manufacture technology of plastic liner of type IV hydrogen storage vessel, Int. J. Hydrog. Energy 47 (13) (2022) 8382–8408.

[4] P. Preuster, A. Alekseev, P. Wasserscheid, Hydrogen storage technologies for future energy systems, Annu. Rev. Chem. Biomol. Eng. 8 (2017), 445e71.

[5] Ahmed M. Elberry, et al., Large-scale compressed hydrogen storage as part of renewable electricity storage systems, Int. J. Hydrog. Energy 46 (29) (2021) 15671–15690.

[6] Joakim Andersson, Stefan Grönkvist, Large-scale storage of hydrogen, Int. J. Hydrog. Energy 44 (23) (2019) 11901–11919.

[7] Abdalla M. Abdalla, et al., Hydrogen production, storage, transportation and key challenges with applications: a review, Energy Convers. Manag. 165 (2018) 602–627.

[8] Sung Chan Kim, Seung Hoon Lee, Kee Bong Yoon, Thermal characteristics during hydrogen fueling process of type IV cylinder, Int. J. Hydrog. Energy 35 (13) (2010) 6830–6835.

[9] Abhilash Suryan, Heuy Dong Kim, Toshiaki Setoguchi, Three dimensional numerical computations on the fast filling of a hydrogen tank under different conditions, Int. J. Hydrog. Energy 37 (9) (2012) 7600–7611.

[10] Jinyang Zheng, et al., High pressure steel storage vessels used in hydrogen refueling station, J. Press. Vessel. Technol. 130 (2008) 1.

[11] Mengxiao Li, et al., Review on the research of hydrogen storage system fast refueling in fuel cell vehicle, Int. J. Hydrog. Energy 44 (21) (2019) 10677–10693.

[12] Alexander Air, Md Shamsuddoha, B. Gangadhara Prusty, A review of Type V composite pressure vessels and automated fibre placement based manufacturing, Compos. Part B Eng. 253 (2023), 110573.

[13] Mohammad Azeem, et al., Application of filament winding technology in composite pressure vessels and challenges: a review, J. Energy Storage 49 (2022), 103468.

[14] Calum P. Fowler, Adrian C. Orifici, Chun H. Wang, A review of toroidal composite pressure vessel optimisation and damage tolerant design for high pressure gaseous fuel storage, Int. J. Hydrog. Energy 41 (47) (2016) 22067–22089.

[15] Iain Staffell, et al., The role of hydrogen and fuel cells in the global energy system, Energy Environ. Sci. 12 (2) (2019) 463–491.

[16] Guangyin Zhen, et al., Anaerobic membrane bioreactor towards biowaste biorefinery and chemical energy harvest: recent progress, membrane fouling and future perspectives, Renew. Sust. Energ. Rev. 115 (2019), 109392.

[17] Dongliang Wang, et al., Development of regulations, codes and standards on composite tanks for on-board gaseous hydrogen storage, Int. J. Hydrog. Energy 44 (40) (2019) 22643–22653.

[18] Tiago Sinigaglia, et al., Production, storage, fuel stations of hydrogen and its utilization in automotive applications-a review, Int. J. Hydrog. Energy 42 (39) (2017) 24597–24611.

[19] Brian David James, et al., Hydrogen Storage System Cost Analysis. No. DOE-SA-0005253, Strategic Analysis Inc., Arlington, VA (United States), 2016.

[20] Mariana Pimenta Alves, et al., A review on industrial perspectives and challenges on material, manufacturing, design and development of compressed hydrogen storage tanks for the transportation sector, Energies 15 (14) (2022) 5152.

[21] Xiulei Wang, et al., Advances on materials design and manufacture technology of plastic liner of type IV hydrogen storage vessel, Int. J. Hydrog. Energy 47 (13) (2022) 8382–8408.

[22] B. Rahul, Dharmahinder Singh Chand, J. Dharani, A comprehensive review on the performance analysis of composite overwrapped pressure vessels, Eng. Appl. Sci. Res. 49 (2) (2022) 272–287.

[23] Roham Rafiee, Amirhesam Salehi, Estimating the burst pressure of a filament wound composite pressure vessel using two-scale and multi-scale analyses, Mech. Adv. Mater. Struct. 30 (13) (2023) 2668–2683.

[24] Anton Popelka, et al., Improvement of aluminum/polyethylene adhesion through corona discharge, J. Phys. D. Appl. Phys. 50 (3) (2016), 035204.

[25] Saeed Mousa, Gap-Yong Kim, A direct adhesion of metal-polymer-metal sandwich composites by warm roll bonding, J. Mater. Process. Technol. 239 (2017) 133–139.

[26] Achim Frick, Markus Rettenberger, Marcel Spadaro, Evaluation of the interfacial adhesion between polymer and metal on polymer-metal hybrids, Polym. Test. 106 (2022), 107448.

[27] Shuaijie Zhao, et al., Manufacturing aluminum/polybutylene terephthalate direct joints by using hot water–treated aluminum via injection molding, Int. J. Adv. Manuf. Technol. 107 (2020) 4637–4644.

[28] S. Villalonga, et al., Composite 700 bar-vessel for on-board compressed gaseous hydrogen storage, in: Proc. of 17th International Conference on Composite Materials, Edinburgh, UK, 2009.

[29] S. Villalonga, et al., Applications of full thermoplastic composite for type IV 70 MPa high pressure vessels, in: International Conference on Composite Materials, 2011.

[30] V. Motaharinejad, et al., Enhancement of adhesion between the polymeric liner and the metallic connector of high-pressure hydrogen storage tank, Int. J. Mater. Form. 14 (2021) 249–260.

[31] Jitender Yadav, P.L. Ramkumar, Ajit Kumar Parwani, A comprehensive review to evaluate the consequences of material, additives, and parameterization in rotational molding, J. Polym. Res. 30 (6) (2023) 231.

[32] Muhuo Yu, et al., The effect of cooling rates on thermal, crystallization, mechanical and barrier properties of rotational molding polyamide 11 as the liner material for high-capacity high-pressure vessels, Molecules 28 (6) (2023) 2425.

[33] Danding Li, et al., Improved balance between dimensional stability, mechanical properties and processability of linear low density polyethylene for rotational molding, J. Appl. Polym. Sci. 140 (29) (2023), e54066.

[34] P.L. Ramkumar, Nikita Gupta, Vrushang Sangani, Experimental investigation on underlying mechanism of LLDPE based rotationally molded biocomposites, J. Nat. Fibers 20 (1) (2023), 2156022.

[35] Mateusz Barczewski, et al., Rotational molding of polylactide (PLA) composites filled with copper slag as a waste filler from metallurgical industry, Polym. Test. 106 (2022), 107449.

[36] Sina Ebnesajjad, Arthur H. Landrock, Adhesives Technology Handbook, William Andrew, 2014.

[37] S.S. Voyutskiĭ, The diffusion theory of adhesion, Rubber Chem. Technol. 33 (3) (1960) 748–756.

[38] Frederick M. Fowkes, Role of acid-base interfacial bonding in adhesion, J. Adhes. Sci. Technol. 1 (1) (1987) 7–27.

[39] William C. Wake, Theories of adhesion and uses of adhesives: a review, Polymer 19 (3) (1978) 291–308.

[40] Arnaud Chiche, Pascal Pareige, Costantino Creton, Role of surface roughness in controlling the adhesion of a soft adhesive on a hard surface, C. R. Acad. Sci. Ser. IV Phys. 1 (9) (2000) 1197–1204.

[41] K.W. Allen, Some reflections on contemporary views of theories of adhesion, Int. J. Adhes. Adhes. 13 (2) (1993) 67–72.

[42] Mingyong Zhou, et al., Direct joining of PP-Al5052 hybrid with high bonding strength by two-step anodization treatment and polymer modification, J. Manuf. Process. 95 (2023) 508–520.

[43] Ruslan Melentiev, et al., Towards decoupling chemical and mechanical adhesion at the electroplated metal/polymer interface via precision surface texturing, Surf. Interfaces 38 (2023), 102875.

[44] Jiajin Li, et al., Dynamic response of metal/polymer bilayer composite with optimized surface porosity by experiment and simulation, J. Mater. Res. Technol. 24 (2023) 1626–1637.

[45] Francesco Lambiase, et al., Repairing aluminum-PEEK hybrid metal-polymer joints made by thermo-mechanical joining, J. Manuf. Process. 93 (2023) 1–14.

[46] Jigao Liu, et al., Review of the surface treatment process for the adhesive matrix of composite materials, Int. J. Adhes. Adhes. 126 (2023), 103446.